Design and Analysis of a Current-Controlled Virtual Synchronous Machine for Weak Grids

Javier Roldán-Pérez*, Adrián González-Cajigas†, Alberto Rodríguez-Cabero*, Milan Prodanovic*, and Pablo Zumel‡
*IMDEA Energy Institute, Madrid, Spain. †Alcalá de Henares University, Madrid, Spain.
‡Carlos III University of Madrid, Spain.

***Abstract*—Emulation of inertia has drawn much attention in recent years due to the growing demand for network services from systems operators. In this scenario, the converter control method Virtual Synchronous Machine (VSM) has gained importance because of its inertial properties. However, in its original form VSMs do not have a current-controller and, therefore, the current-limiting functionality severely restricting their use in industrial applications. The current-controlled version of VSMs (CC-VSMs) removes this restriction. In this paper, a CC-VSM is proposed to interface Voltage Source Converters (VSCs) to weak grids. Dynamic aspects of CC-VSMs have been already studied in the literature. However, in this paper, a simplified small-signal model is derived. It is shown that this model is able to capt the essential dynamics of the CC-VSM. Also, a novel method to calculate the steady-state operating condition is developed. Differences between VSMs and CC-VSMs are highlighted, while robustness of CC-VSMs against parameter variations of the electricity network are studied. The control system improvements were demonstrated firstly in simulation and then on a 15 kVA prototype of a VSM.**

***Index Terms*—Virtual Synchronous Machine, Inertia Emulation, Small-Signal Modelling, Current Controller.**

I. Introduction

The large number of power electronics converters integrated to electricity networks is giving rise to the opportunity to use them to provide additional grid services [1]. In this light the emulation of synchronous machines with VSCs has become an attractive option to meet these demands. This control technique is commonly referred to as VSM and its implementation aspects have drawn much in attention in the recently published literature [2, 3]. Parameter design, current limitation and performance under voltage sags are the most important issues to be addressed [4]. Practical solutions to these issues are needed to promote the use of VSMs and many studies have already been carried out with this respect [5–8].

Direct emulation of synchronous machines (without internal controllers) has been reported in the literature as a promising solution when it comes to mimicking the dynamics of synchronous machines [4, 9]. However, synchronous machine emulation without internal controllers has several drawbacks. First, the current generated by the VSC is not controlled in closed-loop and this is of a paramount importance in the case of voltage sags and other severe voltage disturbances provoking severe over-currents and possibly damaging the VSC [1, 10]. For example, Shuai *et al.* [9] presented a modification to the control system in which the VSM is replaced by a hysteresis controller when an over-current is detected. A different approach was presented by Natarajan and Weiss [11]. In that case a virtual impedance was applied and this provided the current limiting functionality in the case of voltage sags and voltage imbalances without modifying the control system. Other solutions to limit the current without internal controllers can also be found in the literature [8].

The most common approach to the VSM (and VSC in general) implementation is to use an inner current controller plus an outer voltage controller [12, 13]. This solution is appropriate for high-power applications (e.g. HVSC-VSC) where the system voltage and frequency are supported by the VSM. However, voltage control approach is not always necessary for the connection of distributed-generation units and other power electronics devices to distribution networks. In these cases, the application of current-controlled version of VSMs (CC-VSMs) is more adequate [2]. For example, Hirase *et al.* [14] proposed an internal current controller for a VSM. The current reference was obtained by multiplying the voltage generated by the VSM by the inverse model of the connection filter. An alternative was proposed by Younis *et al.* [15] for a single-phase VSM. Internal current controllers have also been proposed for Synchronous Power Controllers (SPCs) [16, 17], that have many similarities with VSMs. The idea of an internal current controller was adapted for a VSM in [18]. Here, the formulation proposed in this work will be used. Even though several authors have already applied current controllers in VSMs, their dynamic aspects and possible differences have been seldom studied [13]. In particular, Mo *et al.* [2] presented a detailed state-space model of a CC-VSM. Differences between VSMs and CC-VSMs were highlighted. Compared to this work, the one presented here presents an alternative small-signal model of a CC-VSM. It is shown that this model is able to capt the essential dynamics, but with a reduced number of variables.

In this paper, a small-signal model of a CC-VSM is presented. This model captures the dynamics of the internal

This work was supported in part by the Community of Madrid Government under the project PRICAM (S2013/ICE-2933), and by the Ministerio de Economía, Comercio y Competitividad, Gobierno de España, and ERDF funds, through the project "EPIIOT - Electrónica de potencia integrada e inteligente para el control y la gestión de la energía en la IIO" (DPI2017-88062-R). It also received funds from the project "SOFTEN: Soluciones para mejorar el funcionamiento de aerogeneradores en redes débiles" (RTC-2017-6074-3) and SOLAR1500 (DPI2017-88505-C2-2-R). Corresponding author phone: +34917371120, e-mail: javier.roldan@imdea.org.

978-1-5386-8330-9/19/$31.00 ©2019 IEEE

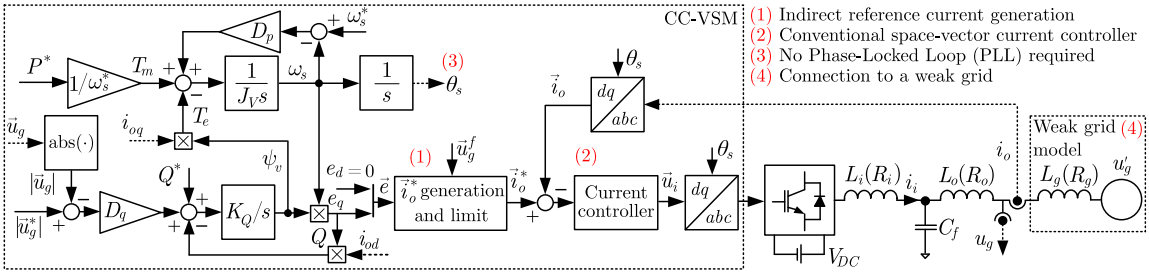

Fig. 1. Electrical diagram of a CC-VSM connected to the grid via an *LCL* filter. The current reference is calculated by using a model of the grid. Park's transformations are calculated by using the virtual shaft angle so that a PLL is not required.

current controller, the reference generation system and the machine emulation in a single state-space representation. An analytic solution is proposed to calculate the steady-state operating condition of the CC-VSM. The model developed here is then applied to analyse the dynamic properties of a CC-VSM connected to a weak grid. In order to highlight the benefits of the internal current controller the dynamic performance of a CC-VSM is compared to that of a VSM. The proposed small-signal model was verified by using firstly simulation and later a 15 kVA prototype of a VSM.

II. System Overview

A. Application Description

Fig. 1 shows the electrical and control system diagrams of a CC-VSM. The VSM (without internal controllers) generates a voltage reference ($\vec{e}$) that is used to generate the reference for the current controller ($\vec{i}_o^*$) [14]. Active power injection is controlled by manipulating the angle of the virtual shaft (θ_s), while reactive power injection (Q) is controlled by manipulating the VSM virtual flux (ψ_v). In a CC-VSM, a current controller is inserted between the VSM and the VSC. The current reference for this controller ($\vec{i}_o^*$) is calculated by using a steady-state model of the connection filter. This model requires the use of the VSM output voltage ($\vec{e}$) and the grid voltage ($\vec{u}_g$). However, the direct use of $\vec{u}_g$ is not recommended since this could amplify noise and generate high-frequency interactions. Therefore, a filtered version of $\vec{u}_g$ ($\vec{u}_g^f$) is used here. Park's transformations are carried out by using the virtual shaft angle (θ_s) so that a PLL is not needed. The converter-side current is $\vec{i}_c$, the grid-side current is $\vec{i}_o$, and the capacitor voltage is $\vec{u}_c$. L_i (R_i), L_o (R_o), and L_g (R_g) are the converter, output, and grid inductance (resistance) values, respectively. C_f is the filter capacitor. Space-vectors will be represented with an arrow over their name (e.g. $\vec{u}_g = u_{gd} + ju_{gq}$). The power-invariant Park's transformation is used to avoid any additional scaling factors [19]. For simplicity, the time dependence of signals will be omitted in the rest of the paper.

B. Current-Controlled Virtual Synchronous Machine

When a CC-VSM is applied, the current reference for the current controller can be calculated as follows [15]:

$$\begin{bmatrix} i_{od}^* \\ i_{oq}^* \end{bmatrix} = K_z \begin{bmatrix} \hat{R}_c & \hat{L}_c\omega_s^* \\ -\hat{L}_c\omega_s^* & \hat{R}_c \end{bmatrix} \begin{bmatrix} e_d - u_{gd}^f \\ e_q - u_{gq}^f \end{bmatrix}, \quad (1)$$

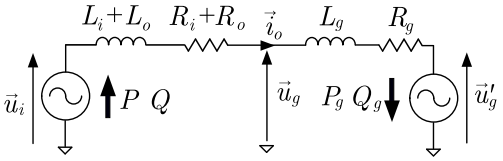

Fig. 2. Simplified electrical diagram used to develop the small-signal model.

where

$$K_z = 1/(\hat{R}_c^2 + \hat{L}_c^2(\omega_s^*)^2), \quad (2)$$

$\hat{L}_c = \hat{L}_i + \hat{L}_o$, and $\hat{R}_c = \hat{R}_i + \hat{R}_o$ are the converter output inductance and resistance, respectively, if the filter capacitor is neglected (see Fig. 2) (hat " ˆ " means "estimated"). A filtered version of $\vec{u}_g$ is used to calculate the reference current in (1) ($\vec{u}_g^f$), and this creates an additional control loop that can have a non-negligible impact on the system dynamics [2].

C. Synchronous Reference Frames Modelling

A synchronous reference frame (DQ) synchronised to the ideal grid voltage space vector ($\vec{u}_g'$) will be used to model the electricity network. However, the VSM will be synchronised to another reference frame (dq) that rotates synchronously with the VSM output voltage ($\vec{e}$). The following transformation is used to refer variables in dq to the DQ reference frame [20]:

$$\begin{bmatrix} f_D \\ f_Q \end{bmatrix} = \begin{bmatrix} \cos\delta_s & -\sin\delta_s \\ \sin\delta_s & \cos\delta_s \end{bmatrix} \begin{bmatrix} f_d \\ f_q \end{bmatrix}, \quad (3)$$

where f refers to an electrical variable (e.g. current or voltage), and δ_s is the angular difference between the angle of the VSM output voltage (θ_s) and that of the ideal grid (θ_g'):

$$\delta_s = \theta_s - \theta_g'. \quad (4)$$

The small-signal model will be presented in the DQ reference frame because a simpler form of analytic expressions is obtained.

III. Current-Controlled VSM Modelling

Fig. 3 shows a diagram of the model developed in this paper. Before linearisation, the state variables are

$$\boldsymbol{x} = [\omega_s \;\; \delta_s \;\; \psi_v \;\; i_{oD} \;\; i_{oQ} \;\; u_{gD}^f \;\; u_{gQ}^f \;\; y_D \;\; y_Q]^T, \quad (5)$$

where T means transposed. The variables u_{gD}^f and u_{gQ}^f are filtered versions of the PCC voltage DQ components, while

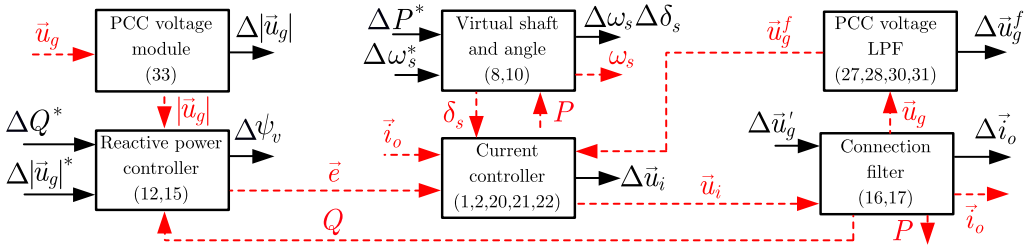

Fig. 3. Calculation of state and intermediate variables of the small-signal model. Blocks indicate a group of calculations to obtain a variable. All the blocks receive the linearised state-space vector ($\Delta\boldsymbol{x}$), while black arrows indicate inputs (references) and outputs (state and intermediate variables). Red arrows indicate physical meaning. Equations used for the calculations are indicated inside the blocks.

y_D and y_Q are the outputs of the current controller integrals. The locks in that figure are explained in the following sections.

A. Virtual Shaft Modelling

The virtual shaft included in the active power controller can be written as follows [21]:

$$J_V \cdot d\omega_s/dt = T_m - T_e - D_p(\omega_s^* - \omega_s), \quad (6)$$
$$d\delta_s/dt = \omega_s - \omega_g, \quad (7)$$

where ω_s and ω_s^* are the synchronous frequency and its reference value, respectively. The electrical torque is $T_e = \psi_v i_{oq}$, the mechanical torque is $T_m = P^*/\omega_s^*$ (P^* is the active power reference), and D_p is the active-power droop coefficient [4]. This equation can be linearised, yielding:

$$J_V \cdot d\Delta\omega_s/dt = \Delta P^*/\omega_s^* - \Delta T_e + D_p(\Delta\omega_s^* - \Delta\omega_s), \quad (8)$$

where "$\Delta(\cdot)$" stands for the incremental operator [22]. The only term in (8) that is non-linear is T_e, and it can written in terms of the DQ reference frame variables:

$$\Delta T_e = \Delta(\psi_v i_{oq}) = \Delta(\psi_v(i_{oQ}\cos\delta_s - i_{oD}\sin\delta_s)). \quad (9)$$

This equation can be linearised, yielding

$$\Delta T_e = \boldsymbol{K}_{T_e} \cdot \Delta\boldsymbol{x}. \quad (10)$$

The gain in (10) can be calculated in terms of the steady-state values of the system state variables.

B. Reactive Power Controller Modelling

The voltage generated by the VSM is applied in the q-axis component of $\vec{e}$, only. Therefore [21]:

$$\vec{e} = 0 + je_q, \quad e_q = \omega_s\psi_v. \quad (11)$$

The state equation generated by the reactive-power controller can be written in its linerised form as follows:

$$d\Delta\psi_v/dt = K_Q \cdot (\Delta Q^* - \Delta Q + \Delta Q_d), \quad (12)$$

where K_Q is the reactive-power controller gain and the term Q_d provides grid voltage support:

$$\Delta Q_d = D_q(\Delta|\vec{u}_g^*| - \Delta|\vec{u}_g|), \quad (13)$$

where D_q is the reactive-power droop coefficient. The equation used to calculate the reactive power generated by the VSM is non-linear ($Q = e_q i_{oq}$). Therefore:

$$\Delta Q = \Delta(\omega_s\psi_v i_{od}) = \\ = \Delta(\omega_s\psi_v(i_{oD}\cos\delta_s + i_{oQ}\sin\delta_s)). \quad (14)$$

By linearising (14), the following expression is obtained:

$$\Delta Q = \boldsymbol{K}_Q \cdot \Delta\boldsymbol{x} + \boldsymbol{G}_Q \cdot \Delta\boldsymbol{u}. \quad (15)$$

where $\boldsymbol{u}$ refers to inputs of the system.

C. Current Controller and Filter Modelling

From Fig. 2, the equations of the connection filter are:

$$L \cdot di_{oD}/dt = u_{iD} - u'_{gD} - R \cdot i_{oD} + L\omega_g i_{oQ}, \quad (16)$$
$$L \cdot di_{oQ}/dt = u_{iQ} - u'_{gQ} - R \cdot i_{oQ} - L\omega_g i_{oD}, \quad (17)$$

where $L = L_i + L_o + L_g$, $R = R_i + R_o + R_g$, and ω_g is the frequency of the ideal grid. Equations (16) and (17) are linear. However, u_{iD} and u_{iQ} connect the VSC output voltage with the electrical circuit. Therefore, u_{iD} and u_{iQ} should be rewritten in terms of the system state variables. First,

$$u_{iD} = u_{id}\cos\delta_s - u_{iq}\sin\delta_s, \quad (18)$$
$$u_{iQ} = u_{id}\sin\delta_s + u_{iq}\cos\delta_s. \quad (19)$$

The dq components of $\vec{u}_i$ are the output signals of the current controller:

$$u_{id} = K_p \cdot (i_{od}^* - i_{od}) + K_p/T_i \cdot y_d + u_{gd} - \hat{L}\omega_s i_{oq}, \quad (20)$$
$$u_{iq} = K_p \cdot (i_{oq}^* - i_{oq}) + K_p/T_i \cdot y_q + u_{gq} + \hat{L}\omega_s i_{od}, \quad (21)$$

where:

$$dy_d/dt = i_{od}^* - i_{od}, \quad dy_q/dt = i_{oq}^* - i_{oq}. \quad (22)$$

The proportional gain and the time constant of the PI controller are K_p and T_i, respectively. The PCC voltage ($\vec{u}_g$) is not a state variable of the system. Therefore, it should be calculated as a function of these. The PCC voltage can be calculated from the electrical circuit equivalent (in any reference frame):

$$\vec{u}_g = \frac{L_g}{L}\vec{u}_i + \frac{L_c}{L}\vec{u}'_g + \left(R_g - \frac{R_c L_g}{L_c}\right)\frac{L_c}{L}\vec{i}_o. \quad (23)$$

Equation (23) is linear and links the PCC voltage with inputs and state variables of the electrical circuit.

D. VSC Output Voltage Small-Signal Model

In order to make use of the small-signal model the VSC output voltage is written in terms of the system state variables and applied as an intermediate variable that connects the current controller with the electrical circuit. This can be done by replacing the following variables in the VSC command signals, (18) and (19): u_{id} and u_{iq} from (20) and (21), $\vec{u}_g$ from (23), and i^*_{od} and i^*_{oq} from (1). This yields the following expressions:

$$u_{iD} = f_{u_{iD}}(\boldsymbol{x}, \boldsymbol{u}), \;\; u_{iQ} = f_{u_{iQ}}(\boldsymbol{x}, \boldsymbol{u}), \tag{24}$$

where $f_{u_{iD}}(\cdot,\cdot)$ and $f_{u_{iQ}}(\cdot,\cdot)$ are functions of the system parameters. These functions can be linearised, giving:

$$\Delta u_{iD} = \boldsymbol{K}_{u_{iD}} \cdot \Delta \boldsymbol{x} + \boldsymbol{G}_{u_{iD}} \cdot \Delta \boldsymbol{u}, \tag{25}$$

$$\Delta u_{iQ} = \boldsymbol{K}_{u_{iQ}} \cdot \Delta \boldsymbol{x} + \boldsymbol{G}_{u_{iQ}} \cdot \Delta \boldsymbol{u}. \tag{26}$$

E. Grid voltage filter

A first-order low-pass filter (LPF) is applied to each of the PCC voltage components in order to calculate the reference current. This can be written as:

$$du^f_{gD}/dt = (u_{gD} - u^f_{gD}) \cdot \omega_c, \tag{27}$$

$$du^f_{gQ}/dt = (u_{gQ} - u^f_{gQ}) \cdot \omega_c, \tag{28}$$

where ω_c is the cut-off frequency of the LPF. First, the value of u_g in (23) should be replaced in (20) and (21). Then, i^*_{od} and i^*_{oq} should be replaced by using (1). This result is then replaced in (27) and (28), yielding

$$u^f_{gD} = f_{u^f_{gD}}(\boldsymbol{x}, \boldsymbol{u}), \;\; u^f_{gQ} = f_{u^f_{gQ}}(\boldsymbol{x}, \boldsymbol{u}), \tag{29}$$

where $f_{u^f_{gD}}(\cdot,\cdot)$ and $f_{u^f_{gQ}}(\cdot,\cdot)$ are functions of the system parameters. These equations can be linearised, giving:

$$\Delta u^f_{gD} = \boldsymbol{K}_{u^f_{gD}} \cdot \Delta \boldsymbol{x} + \boldsymbol{G}_{u^f_{gD}} \cdot \Delta \boldsymbol{u}, \tag{30}$$

$$\Delta u^f_{gQ} = \boldsymbol{K}_{u^f_{gQ}} \cdot \Delta \boldsymbol{x} + \boldsymbol{G}_{u^f_{gQ}} \cdot \Delta \boldsymbol{u}. \tag{31}$$

F. Grid Voltage Module Model

The module of the PCC-voltage space vector is used in the VSM to provide grid voltage support. This variable is not a state variable of the system and it is included in the model to simplify expressions and retain their physical meaning:

$$|\vec{u}_g| = \sqrt{u^2_{gD} + u^2_{gQ}}. \tag{32}$$

The linearised version of (32) can be written as follows:

$$\Delta|\vec{u}_g| = \boldsymbol{K}_{u_g} \cdot \Delta \boldsymbol{x} + \boldsymbol{G}_{u_g} \cdot \Delta \boldsymbol{u}. \tag{33}$$

G. Complete Model and State-Space Representation

All the equations of the small-signal model developed in this paper can be written as a state-space representation:

$$d/dt\Delta \boldsymbol{x} = \boldsymbol{A} \cdot \Delta \boldsymbol{x} + \boldsymbol{B}^* \cdot \Delta \boldsymbol{u}^* + \boldsymbol{B}^d \cdot \Delta \boldsymbol{u}^d, \tag{34}$$

where

$$\boldsymbol{u}^* = [P^* \;\; Q^* \;\; |\vec{u}^*_g| \;\; \omega^*_s]^T, \;\; \boldsymbol{u}^d = [u'_{gD} \;\; u'_{gQ}]^T, \tag{35}$$

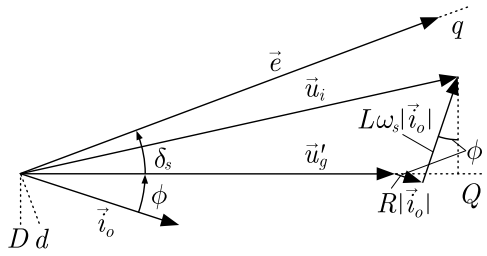

Fig. 4. Representation of the steady-state space vectors for the CC-VSM.

$\boldsymbol{A}$ is the system state matrix, $\boldsymbol{B}^*$ is the matrix of reference inputs, and $\boldsymbol{B}^d$ is the matrix of disturbances. In addition, the small-signal model can be used for simulation by following the structure depicted in Fig. 3.

IV. Operating-Point Calculation

The operating point can be calculated by numerically solving the CC-VSM non-linear equations. However, an explicit solution would facilitate the analysis and, having this in mind, the ideal grid voltage ($\vec{u}'_g$) and the active (P_g) and reactive (Q_g) powers injected to the ideal grid are taken as inputs. The method proposed in this paper is based on the classical method used for synchronous generators [23], but it has been adapted for CC-VSMs.

The VSM frequency must be equal to the grid frequency in steady-state, because the latter is fixed. Therefore:

$$\omega^o_s = \omega_g. \tag{36}$$

Since the active and reactive powers injected to the ideal grid are taken as inputs, the steady-state value of the output current can be easily obtained. From Fig. 4:

$$\vec{i}_o = i_{oD} + j \cdot i_{oQ} = |\vec{i^{\,o}_o}|(\sin\phi^o + j\cos\phi^o), \tag{37}$$

where:

$$|\vec{i^{\,o}_o}| = \sqrt{(P^o_g)^2 + (Q^o_g)^2}/|\vec{u}'^o_g|, \tag{38}$$

$$\phi^o = \cos^{-1}\left(P^o_g/\sqrt{(P^o_g)^2 + (Q^o_g)^2}\right). \tag{39}$$

Once the current is known, the PCC voltage can be calculated with the equation of the PCC voltage, giving:

$$u^o_{gD} = u'^o_{gD} + R_g i^o_{oD} - L_g \omega^o_s i^o_{oQ}, \tag{40}$$

$$u^o_{gQ} = u'^o_{gQ} + R_g i^o_{oQ} + L_g \omega^o_s i^o_{oD}. \tag{41}$$

The LPF used to filter the PCC voltage does not modify the steady-state condition since it has unitary gain. Now, in order to calculate the voltage generated by the VSM, the equation used to calculate the reference current, (1), can be referred to the DQ reference frame. In this case, the DQ components of $\vec{e}^{\,o}$ can be calculated as follows:

$$\begin{bmatrix} e^o_D \\ e^o_Q \end{bmatrix} = \begin{bmatrix} \hat{R}_c & -\omega^*_s \hat{L}_c \\ \omega^*_s \hat{L}_c & \hat{R}_c \end{bmatrix} \begin{bmatrix} i^o_{oD} \\ i^o_{oQ} \end{bmatrix} + \begin{bmatrix} u^o_{gD} \\ u^o_{gQ} \end{bmatrix}. \tag{42}$$

The control system includes a PI controller over the output current. Therefore, $\vec{i}^{\,o*}_o = \vec{i}^{\,o}_o$ in (42) (in DQ). In (42), it is worth recalling that the hat stands for estimated value.

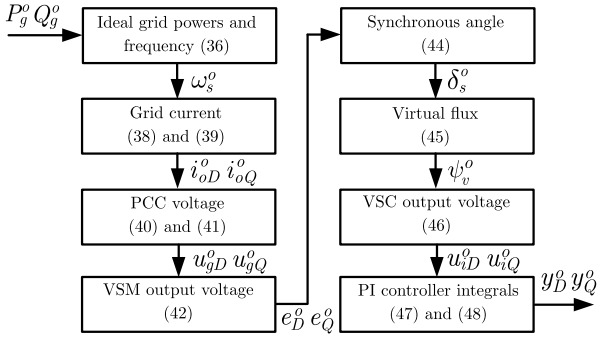

Fig. 5. Proposed procedure to calculate the steady-state condition of the CC-VSM, directly.

The output voltage of the VSM is applied to the q component of the dq reference frame, only. Therefore:

$$e_D^o = -e_q^o \sin\delta_s^o, \quad e_Q^o = e_q^o \cos\delta_s^o. \tag{43}$$

From (43), the value of the δ_s^o can be obtained:

$$\delta_s^o = -\tan^{-1}(e_D^o/e_Q^o). \tag{44}$$

With δ_s^o already found, the virtual flux can be calculated from its definition in (11), yielding:

$$\psi_v^o = e_Q^o/(\omega_s^o \cdot \cos\delta_s^o). \tag{45}$$

The steady-state values of the current controller integrals are required for the small-signal model and, in order to calculate them, the voltage generated by the VSC is also required. The latter can be calculated by using the electrical equations of the CC-VSM, thus

$$\begin{bmatrix} u_{iD}^o \\ u_{iQ}^o \end{bmatrix} = \begin{bmatrix} R & -\omega_s^o L \\ \omega_s^o L & R \end{bmatrix} \begin{bmatrix} i_{oD}^o \\ i_{oQ}^o \end{bmatrix} + \begin{bmatrix} u'^o_{gD} \\ u'^o_{gQ} \end{bmatrix}. \tag{46}$$

After this step, the integrals of the current controller can be solved from (20) and (21), yielding:

$$y_D^o = T_i/K_p \cdot (u_{iD}^o - u_{gD}^o + \hat{L}\omega_s^o i_{oQ}^o), \tag{47}$$

$$y_Q^o = T_i/K_p \cdot (u_{iQ}^o - u_{gQ}^o - \hat{L}\omega_s^o i_{oD}^o). \tag{48}$$

A coupling term appears when $\vec{u}_i$ is transformed from the dq to the DQ reference frame due to the transformation of $d\vec{y}/dt = \vec{i}_o^* - \vec{i}_o$. However, the PI controller forces the fundamental component $\vec{i}_o^o = \vec{i}_o^{*o}$ and then the coupling term disappears in steady state.

Fig. 5 shows a diagram with the procedure proposed to calculate the steady-state condition. The main benefit of this method is that no iterative calculations are required. This is a novel contribution of this paper.

V. Case Study and Prototype Description

The nominal voltage of the grid was 400 V and the nominal frequency 50 Hz. The *LCL* filter values were $L_i = 2.3$ mH, $L_o = 0.93$ mH, and $C_f = 8.8$ μF. The VSM parameters were $J_V = 0.5$ and $D_p = 8$. This design provided overshoot for stiff grids. The gain of the voltage controller was set to $K_Q = 1.5 \cdot 10^{-3}$, while $D_q = 50$. The crossover frequency of the current was set to $250{\cdot}2\pi$ rad/s. Classical decoupling terms and PCC voltage feed-forward were applied [24]. The VSM was implemented as suggested in [25]. The sampling and switching frequencies were made equal to 10 kHz. PWM with single update and third-harmonic injection was used [24]. Current controller integrals were discretised by using the backward Euler method [22]. Notch filters at the harmonic frequencies were used in the VSM command so that harmonic components coming from the VSM were eliminated [21].

A 15 kVA VSC was used to carry out the experiments. The grid was emulated by using another converter operated in open-loop. The nominal grid inductance was $L_g = 2.3$ mH. Weak grid conditions were emulated by inserting inductors between the VSM and the grid emulator. More details of the laboratory facilities can be found in [26, 27].

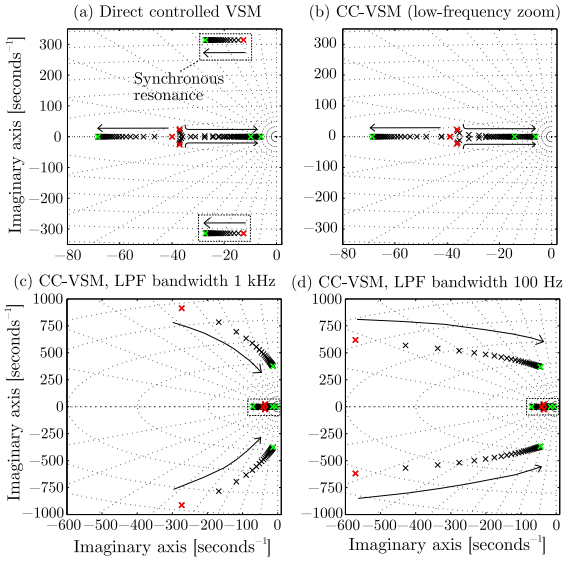

Fig. 6. Pole-zero diagram of the (a) conventional VSM, and (b,c,d) CC-VSM, for the same parameters. In all the figures the grid inductance varies between 0 and 0.5 pu. In (c,d), CC-VSM, where the bandwidth of the LPF is (c) 1 kHz and (d) 100 Hz.

VI. Analytic Study

The performance of the CC-VSM was analysed for weak-grid scenarios. Also, it was compared to that of a VSM without internal controllers in order to highlight differences. The small-signal model of the VSM was obtained by using a procedure similar to the one proposed for the CC-VSM in this paper.

A. Grid Impedance Effect

Fig. 6 (a) shows the pole-zero diagram of the conventional VSM when the value of the grid inductance increases. There are three low-frequency poles, which correspond to the virtual shaft (two complex poles) and the voltage controller (one single pole). When the grid inductance increases, the two complex poles moved towards the real axis, until they reached it. Then, the poles moved towards the imaginary axis. On the other hand, the single pole related to the voltage controller increases its frequency. In addition to these poles, there are

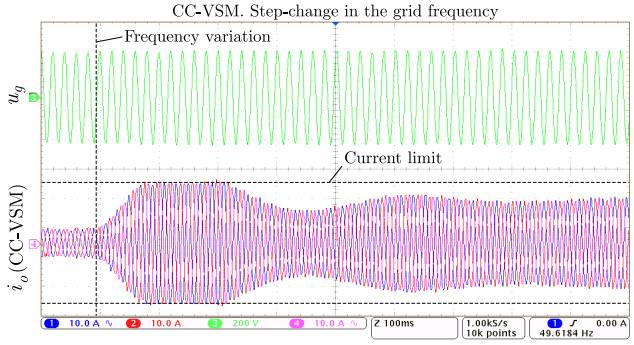

Fig. 7. Experimental results for a CC-VSM connected to a weak grid. Grid voltage (u_g) and output current (i_o) for a step-change of the grid frequency.

two complex poles that have a module close to the synchronous frequency (ω_s). These poles generate a resonance that is commonly known as "synchronous resonance", and it appears because of the coupling terms present in the dynamic equations of the connection filter [2, 28]. The damping factor and frequency of these poles increase together with the grid inductance value.

Fig. 6 (b) shows the pole-zero diagram of the CC-VSM. The low-frequency poles are similar to those of a VSM. However, in the CC-VSM the synchronous resonance does not appear. This is because the current controller includes decoupling terms that cancel the coupling terms of the connection filter. When L_g increases, the low-frequency poles of both methods have a similar trend.

B. Low-Pass Filter Effect

Fig. 6 (c) shows the pole-zero diagram of the CC-VSM when the bandwidth of the low-pass filter is set to 1 kHz, while Fig. 6 (d) shows the same figure, but for a bandwidth of 100 Hz. The low-frequency poles have a similar trend for the two cases. However, the high-frequency poles approach faster the imaginary axis when the LPF bandwidth is larger. This will generate oscillations in the controlled variables and noise amplification. Therefore, it is clear the LPF design has a considerable impact on the system dynamics. These results agree with other dynamic studies of CC-VSMs already presented in the literature [2].

VII. Results

Fig. 7 shows the experimental results obtained when the CC-VSM was connected to the grid and the frequency suddenly decreased. The instant in which the frequency changed is marked in the figure. Initially, the CC-VSM was working in steady-state. When the frequency changed, the CC-VSM supplied the active power required to support the grid. However, the current saturated during the transient to avoid the converter damage. This was possible because of the saturation included within the current controller.

Fig. 8 shows the simulation results for active and reactive powers injected by (blue) the VSM and (red) the CC-VSM, for a step-change of Q^*. The synchronous resonance clearly

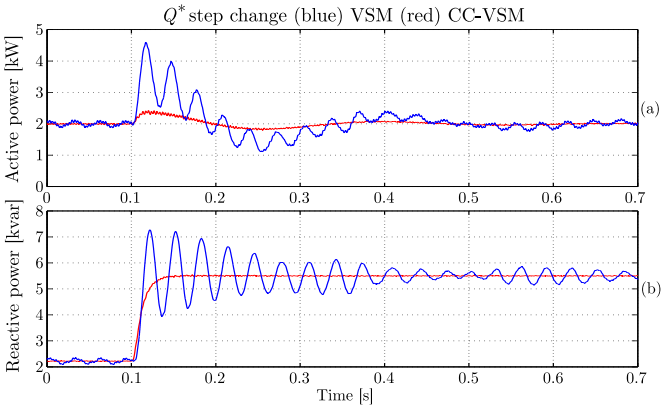

Fig. 8. Active and reactive power flows for (blue) VSM and (red) CC-VSM, for the same control parameters applied.

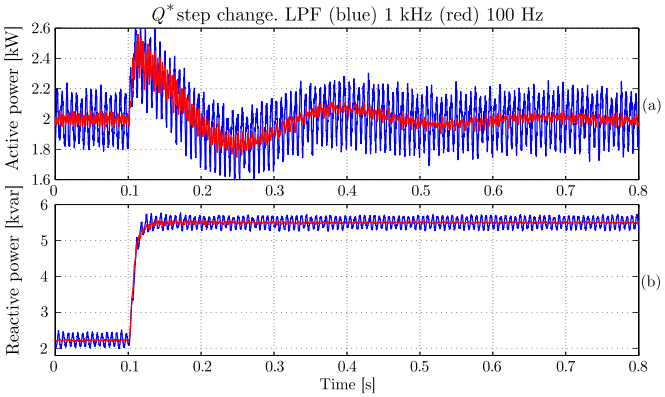

Fig. 9. Active and reactive power flows for a CC-VSM with LPF bandwidths of (red) 100 Hz and (blue) 1 kHz.

affected the VSM performance. However, this effect was not present in the CC-VSM. These results are in agreement with the theoretical results obtained by using the small-signal analysis.

Fig. 9 shows the transient response of the CC-VSM when the LPF bandwidth was (blue) 1 kHz and (red) 100 Hz. In both cases, the mean value of the reactive power reached quickly its steady-state value. However, when the LPF bandwidth was set to 1 kHz, active and reactive power showed high-frequency oscillations. These oscillations were clearly reduced when the bandwidth of the filter was set to 100 Hz. This result highlights the importance of reducing the LPF bandwidth to avoid high-frequency interactions between the current controller and the reference generation system.

VIII. Conclusion

In this paper a detailed small-signal model of a CC-VSM has been developed. All dynamic equations of the CC-VSM have been introduced, explained and then linearised. An analytic procedure to calculate the steady-state condition of the CC-VSM has been proposed, and this is a contribution of this paper. Finally, the small-signal model developed in this paper has been used to analyse the dynamics of a CC-VSM

connected to a weak grid. In order to highlight the benefits of internal current controllers a critical comparison between the CC-VSM and the VSM was performed.

Results revealed that a CC-VSM is a robust control alternative for the connection of VSCs to weak grids. Also, one of the most important conclusions is that the use of a current controller helps suppressing the synchronous resonance present in VSMs. This represents a clear advantage over direct emulation of synchronous machines. The impact of the weak grid was also examined and it was demonstrated that the synchronous resonance effect is reduced for large values of the grid impedance when direct emulation (no internal controllers) is used. Also, the VSM becomes more damped and slower when the grid inductance increases. The effect of the LPF used to calculate the current reference in CC-VSMs was also explored. It was shown that the bandwidth of this filter can a have a significant impact on the closed-loop stability, especially in weak-grid scenarios. The results obtained with the model developed in this work agree with the ones already obtained in the literature by using other models [2].

The modelling and control system developments were validated firstly in simulation and then on a 15 kW prototype of a VSM connected to weak-grid.

REFERENCES

[1] J. Roldán-Pérez, A. García-Cerrada, J. L. Zamora-Macho, and M. Ochoa-Giménez, "Helping all generations of photo-voltaic inverters ride-through voltage sags," *IET Power Electronics*, vol. 7, no. 10, pp. 2555–2563, 2014.

[2] O. Mo, S. D'Arco, and J. A. Suul, "Evaluation of virtual synchronous machines with dynamic or quasi-stationary machine models," *IEEE Transactions on Industrial Electronics*, vol. PP, no. 99, pp. 1–1, 2016.

[3] H. A. Alsiraji and R. El-Shatshat, "Comprehensive assessment of virtual synchronous machine based voltage source converter controllers," *IET Generation, Transmission Distribution*, vol. 11, no. 7, pp. 1762–1769, 2017.

[4] Q. C. Zhong and G. Weiss, "Synchronverters: Inverters that mimic synchronous generators," *IEEE Transactions on Industrial Electronics*, vol. 58, no. 4, pp. 1259–1267, April 2011.

[5] Z. Shuai, W. Huang, C. Shen, J. Ge, and Z. J. Shen, "Characteristics and restraining method of fast transient inrush fault currents in synchronverters," *IEEE Transactions on Industrial Electronics*, vol. 64, no. 9, pp. 7487–7497, Sept 2017.

[6] S. D'Arco, J. A. Suul, and O. B. Fosso, "A virtual synchronous machine implementation for distributed control of power converters in smartgrids," *Electric Power Systems Research*, vol. 122, pp. 180–197, 2015.

[7] H. Zhao, Q. Yang, and H. Zeng, "Multi-loop virtual synchronous generator control of inverter-based dgs under microgrid dynamics," *IET Generation, Transmission Distribution*, vol. 11, no. 3, pp. 795–803, 2017.

[8] S. Dong, Y. Chi, and Y. Li, "Active voltage feedback control for hybrid multiterminal HVDC system adopting improved synchronverters," *IEEE Transactions on Power Delivery*, vol. 31, no. 2, pp. 445–455, April 2016.

[9] Z. Shuai, W. Huang, C. Shen, J. Ge, and Z. J. Shen, "Characteristics and restraining method of fast transient inrush fault currents in synchronverters," *IEEE Trans. on Ind. Elec.*, vol. 64, no. 9, pp. 7487–7497, Sept 2017.

[11] V. Natarajan and G. Weiss, "Synchronverters with better stability due to virtual inductors, virtual capacitors, and anti-windup," *IEEE Trans. on Industrial Electronics*, vol. 64, no. 7, pp. 5994–6004, July 2017.

[10] M. A. G. López, J. L. G. de Vicuña, J. Miret, M. Castilla, and R. Guzmán, "Control strategy for grid-connected three-phase inverters during voltage sags to meet grid codes and to maximize power delivery capability," *IEEE Transactions on Power Electronics*, vol. 33, no. 11, pp. 9360–9374, Nov 2018.

[12] S. D'Arco, J. A. Suul, and O. B. Fosso, "Small-signal modeling and parametric sensitivity of a virtual synchronous machine in islanded operation," *Int. Jou. of Elec. Power & Energy Systems*, vol. 72, pp. 3–15, 2015.

[13] ——, "Automatic tuning of cascaded controllers for power converters using eigenvalue parametric sensitivities," *IEEE Trans. on Ind. App.*, vol. 51, no. 2, pp. 1743–1753, March 2015.

[14] Y. Hirase, K. Sugimoto, K. Sakimoto, and T. Ise, "Analysis of resonance in microgrids and effects of system frequency stabilization using a virtual synchronous generator," *IEEE Journal of Emerging and Selected Topics in Power Electronics*, vol. 4, no. 4, pp. 1287–1298, Dec 2016.

[15] T. Younis, M. Ismeil, E. K. Hussain, and M. Orabi, "Single-phase self-synchronized synchronverter with current-limiting capability," in *2016 Eighteenth International Middle East Power Systems Conference (MEPCON)*, Dec 2016, pp. 848–853.

[16] W. Zhang, A. M. Cantarellas, J. Rocabert, A. Luna, and P. Rodriguez, "Synchronous power controller with flexible droop characteristics for renewable power generation systems," *IEEE Transactions on Sustainable Energy*, vol. 7, no. 4, pp. 1572–1582, Oct 2016.

[17] M. Reyes, P. Rodriguez, S. Vazquez, A. Luna, R. Teodorescu, and J. M. Carrasco, "Enhanced decoupled double synchronous reference frame current controller for unbalanced grid-voltage conditions," *IEEE Transactions on Power Electronics*, vol. 27, no. 9, pp. 3934–3943, Sept 2012.

[18] J. Roldan-Perez, A. Rodriguez-Cabero, and M. Prodanovic, "Parallel current-controlled synchronverters for voltage and frequency regulation in weak grids," in *9th International Conference on Power Electronics, Machines and Drives (PEMD 2018)*, Apr 2018.

[19] P. C. Krause, O. Wasynczuk, and S. D. Sudhoff, *Analysis of Electric Machinery and Drive Systems*, 2nd ed. Wiley-IEEE Press, Feb. 2002.

[20] A. Rodríguez-Cabero, M. Prodanovic, and J. Roldán-Pérez, "Analysis of dynamic properties of vscs connected to weak grids including the effects of dead-time and time delays," *IEEE Transactions on Sustainable Energy*, pp. 1–1, 2018.

[21] J. Roldán-Pérez, A. Rodríguez-Cabero, and M. Prodanovic, "Harmonic virtual impedance design for parallel-connected grid-tied synchronverters," *IEEE Journal of Emerging and Selected Topics in Power Electronics*, pp. 1–1, 2018.

[22] B. Kuo, *Digital Control Systems*. Oxford University Press, 1992.

[23] P. Kundur, N. Balu, and M. Lauby, *Power system stability and control*, ser. EPRI power system engineering series. McGraw-Hill, 1994.

[24] J. Roldán-Pérez, E. J. Bueno, R. Pena-Alzola, and A. Rodríguez-Cabero, "All-pass-filter-based active damping for vscs withlclfilters connected to weak grids," *IEEE Transactions on Power Electronics*, vol. 33, no. 11, pp. 9890–9901, Nov 2018.

[25] J. Roldán-Pérez, M. Prodanovic, and A. Rodríguez-Cabero, "Detailed discrete-time implementation of a battery-supported synchronverter for weak grids," in *43rd Annual Conference of the IEEE Industrial Electronics Society (IECON)*, November 2017.

[26] M. Prodanovic, A. Rodríguez-Cabero, M. Jiménez-Carrizosa, and J. Roldán-Pérez, "A rapid prototyping environment for DC and AC microgrids: Smart Energy Integration Lab (SEIL)," in *2017 IEEE Second Int. Conf. on DC Microgrids (ICDCM)*, June 2017, pp. 421–427.

[27] F. Huerta, J. K. Gruber, M. Prodanovic, and P. Matatagui, "Power-hardware-in-the-loop test beds: evaluation tools for grid integration of distributed energy resources," *IEEE Industry Applications Magazine*, vol. 22, no. 2, pp. 18–26, March 2016.

[28] L. Zhang, L. Harnefors, and H. Nee, "Power-synchronization control of grid-connected voltage-source converters," *IEEE Transactions on Power Systems*, vol. 25, no. 2, pp. 809–820, May 2010.